Journal of ELECTRONIC MATERIALS, Vol. 39, No. 4, 2010
DOI: 10.1007/s11664-010-1140-5
© 2010 TMS

Growth and Characterization of Unintentionally Doped GaSb Nanowires

ROBERT A. BURKE,[1] XIAOJUN WENG,[2] MENG-WEI KUO,[3] YOUNG-WOOK SONG,[4] ANNE M. ITSUNO,[3] THERESA S. MAYER,[2,3] STEVEN M. DURBIN,[5] ROGER J. REEVES,[4] and JOAN M. REDWING[1,2,3,6]

1.—Department of Materials Science and Engineering, The Pennsylvania State University, University Park, PA 16802, USA. 2.—Materials Research Institute, The Pennsylvania State University, University Park, PA 16802, USA. 3.—Department of Electrical Engineering, The Pennsylvania State University, University Park, PA 16802, USA. 4.—Department of Physics and Astronomy, University of Canterbury, Christchurch 8140, New Zealand. 5.—Department of Electrical and Computer Engineering, University of Canterbury, Christchurch 8140, New Zealand. 6.—e-mail: jmr31@psu.edu

GaSb nanowires were synthesized on *c*-plane sapphire substrates by gold-mediated vapor–liquid–solid (VLS) growth using a metalorganic chemical vapor deposition process. A narrow process window for GaSb nanowire growth was identified. Chemical analysis revealed variations in the catalyst composition which were explained in terms of the Au-Ga-Sb ternary phase diagram and suggest that the VLS growth mechanism was responsible for the nanowire growth. The nominally undoped GaSb nanowires were determined to be *p*-type with resistivity on the order of 0.23 Ω cm. The photoluminescence was found to be highly dependent on the V/III ratio, with an optimal ratio of unity.

Key words: MOCVD, GaSb, nanowires

INTRODUCTION

GaSb nanowires are of interest for a variety of applications, including high-speed electronics,[1] mid-infrared optoelectronics,[2] and thermoelectrics.[3] Interest in these applications is due to the high hole mobility of GaSb (850 $cm^2/V\ s$)[4] and the ability to bandgap-engineer GaSb (0.7 eV) with InSb (0.17 eV) and AlSb (1.6 eV).[5] To date, however, a limited number of studies have been carried out to investigate the growth and properties of GaSb nanowires compared with other III–V materials. GaSb nanowires have been synthesized by a focused ion beam technique,[6] direct antimonidization/reactive vapor transport,[7] and cold-wall metalorganic chemical vapor deposition (MOCVD).[8–10]

MOCVD is of particular interest since it is used for commercial device fabrication and enables the ability to control doping and alloy composition during growth. Previous MOCVD studies have focused on growth of GaSb/GaAs nanowire heterostructures.[8–10] In these studies, the GaSb segments were observed to be significantly larger in diameter than the GaAs segments, and the GaSb nanowire growth rate was also noted to be much lower than that of the GaAs segment, on the order of 2 nm/min to 30 nm/min.[8,10] While initial studies were also completed investigating the optical and electrical properties of the GaSb nanowires,[9] the low growth rates are generally problematic for the fabrication of longer nanowires which are typically needed for electrical testing.

In this study, GaSb nanowires were synthesized by metal-mediated vapor–liquid–solid (VLS) growth using a hot-wall MOCVD reactor at higher precursor mole fractions, which enabled an increase in the nanowire growth rate. The effects of growth conditions on the structural properties of the nanowires were investigated, and the chemical composition of the catalyst was determined by x-ray energy-dispersive spectroscopy (XEDS) in a scanning transmission electron microscope (STEM). Photoluminescence (PL) measurements were carried out to determine the optical properties of the nanowires.

(Received September 9, 2009; accepted February 13, 2010; published online March 11, 2010)

The nanowire resistivity and carrier type were determined from four-point measurements of individual nanowires using a back-gated test structure.

EXPERIMENTAL PROCEDURES

GaSb nanowires were synthesized in an isothermal quartz tube reactor using trimethylgallium [$(CH_3)_3Ga$, TMGa] and trimethylantimony [$(CH_3)_3Sb$, TMSb] as group III and V precursors, respectively, and purified hydrogen (H_2) as the carrier gas. *c*-Plane sapphire substrates were functionalized with 3-aminopropyltrimethoxysilane (Gelest, Inc., Morrisville, PA) prior to applying a gold colloid solution consisting of 50-nm nanoparticles (Ted Pella, Inc., Redding, CA). The samples were loaded into the reactor in a quartz boat and heated to the growth temperature in 100 sccm H_2 (total flow rate: 140 sccm). For the nanowire growths, the TMGa and TMSb precursors were maintained at temperatures of −10°C and 4°C, respectively, and were held at pressure of 760 Torr. The effects of growth temperature (450°C to 550°C), reactor pressure (13 Torr to 600 Torr), V/III ratio (0.5 to 2), TMGa flow rate (0.66 sccm to 2 sccm), and TMSb flow rate (0.66 sccm to 2 sccm) were studied in order to determine a suitable process window for nanowire growth. Typical growth times were on the order of 5 min to 10 min.

Structural characterization and compositional analysis of the GaSb nanowires were performed using scanning electron microscopy (SEM), STEM, and XEDS. SEM (FEI-Philips XL20) was used for plan-view imaging of the as-grown samples. Structural and chemical characterization of released wires was carried out in a JEOL 2010F field-emission TEM/STEM operated at 200 keV. TEM specimens were prepared by sonicating the samples in isopropyl alcohol for 30 s to release the wires from the substrate and then dispersing the solution onto lacey carbon films. In order to investigate the optical properties, temperature- and power-dependent PL measurements were carried out on GaSb nanowires still attached to the *c*-plane sapphire substrates. These studies were performed utilizing an argon laser with a 488 nm excitation wavelength coupled with an Acton SpectraPro 2150i and InSb detector.

Electrical characterization was carried out using a back-gated electrical test-bed structure including four topside electrodes. The two internal electrodes serve as voltage probes for four-point resistance measurements and as source (S) and drain (D) electrodes for gate-dependent measurements. The as-grown GaSb nanowires were released from the substrate by ultrasonic agitation and suspended in isopropyl alcohol for electrical characterization. Samples were fabricated by integrating the nanowires onto n^{++}-Si substrates coated with 110 nm of low-pressure chemical vapor deposition-grown silicon nitride (Si_3N_4) and with 20 nm/60 nm of Ti/Au, which serve as the back-gate dielectric and bottom electrodes, respectively. The individual nanowires were aligned between pairs of electrodes by electrofluidic assembly.[11] Top electrodes were defined by electron-beam lithography (LEICA EBPG-HR) followed by lift-off of thermally evaporated Ti (100 nm)/Au (100 nm). Prior to electrode metallization, the native oxide was removed by diluted HCl ($HCl:H_2O$ = 0.3:100).[12] The separation between the S and D electrodes varied from 1.6 μm to 2.6 μm.

RESULTS AND DISCUSSION

Nanowire Growth

In order to define a suitable process window for GaSb nanowire growth, a series of experiments were conducted to investigate the effects of temperature, pressure, and V/III ratio on the density and structural properties of the nanowires. The results from the temperature and V/III studies will be discussed here, while the pressure study has been reported elsewhere.[13] To examine the effect of growth temperature, the furnace temperature setpoint was varied over the range of 450°C to 550°C at a reactor pressure of 100 Torr. The TMGa and TMSb flow rates were maintained at 1 sccm each (V/III = 1). Nanowire growth was observed over a temperature range of 475°C to 525°C under these conditions (Fig. 1b–d). Large GaSb crystallites were also present over this temperature regime, as indicated by blue arrows in Fig. 1b.

At temperatures below 475°C, the only deposits present on the sapphire substrates were the 50-nm Au nanoparticles that had been applied prior to growth (Fig. 1a). It is believed that the absence of nanowire growth below 475°C is due to insufficient decomposition of the precursors at these process conditions. Nanowires grown at a temperature of 475°C were found to be uniform in diameter (Fig. 1b), while tapering of the nanowires became more prevalent with increasing temperature. This effect was expected due to competing thin-film deposition on the side facets of the nanowires during growth. The presence of competing thin-film deposition is evident at a growth temperature of 525°C, where discontinuities can be observed in the underlying thin film on the substrate (Fig. 1d). Increasing the temperature to 550°C led to large particle deposits on the sapphire surface. Utilizing EDS, the particles were confirmed to consist of Ga and Sb. A temperature of 550°C appears to be too high for nanowire growth, since the operating conditions are approaching those that are commonly used for thin-film deposition of GaSb.[5,14,15] These findings are further supported by cold-wall MOCVD studies where a temperature range of 410°C to 510°C was utilized for GaSb nanowire growth.[8,10]

Higher-magnification SEM images of the GaSb nanowires were obtained in order to measure the length of the nanowires and determine the growth rate for wires grown in the temperature range of

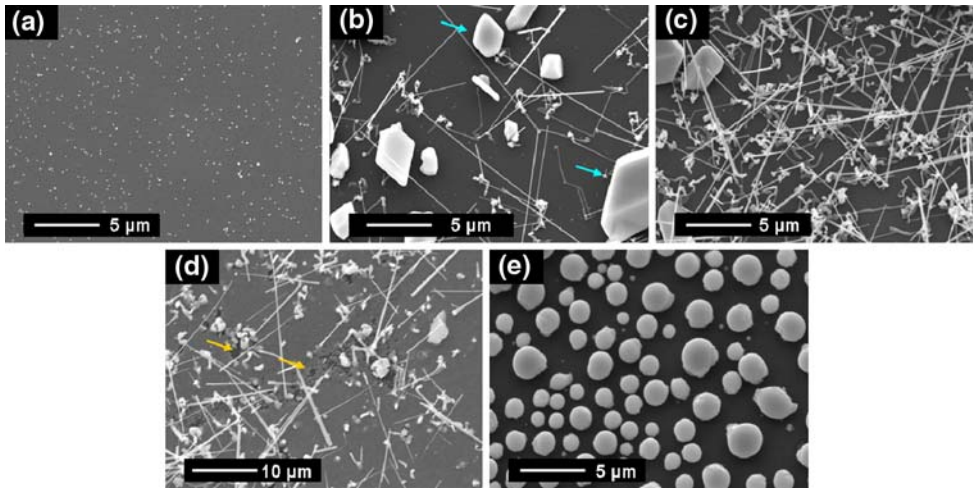

Fig. 1. SEM images of GaSb nanowires grown at temperatures of (a) 450°C, (b) 475°C, (c) 500°C, (d) 525°C, and (e) 550°C. Blue arrows in (b) indicate GaSb crystallites. Orange arrows in (d) indicate discontinuities in the underlying film. Growth conditions: 100 Torr, 1 sccm TMGa, 1 sccm TMSb, 100 sccm H_2, and 5 min growth.

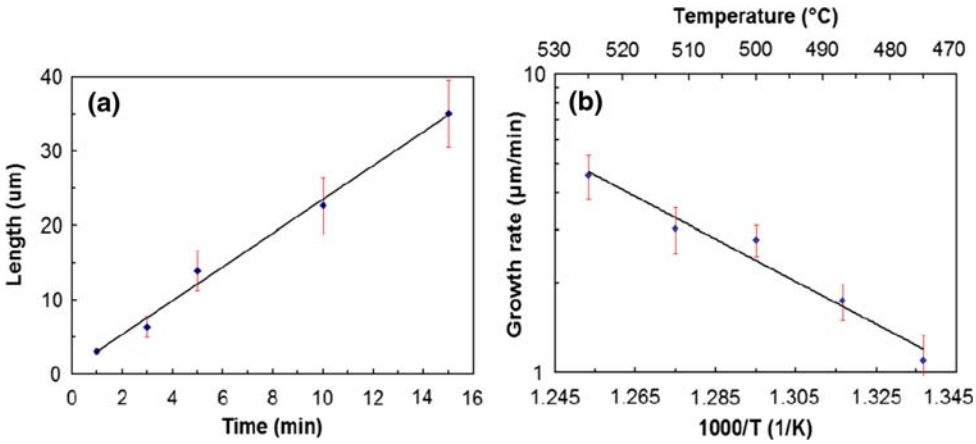

Fig. 2. (a) Length of GaSb nanowires as a function of growth time for GaSb nanowires grown at 500°C. (b) Arrhenius plot of GaSb nanowire growth rate over a temperature range of 475°C to 525°C. Growth conditions: 100 Torr, 1 sccm TMGa, 1 sccm TMSb, and 100 sccm H_2.

475°C to 525°C. The average length of the GaSb nanowires as a function of time is plotted in Fig. 2a for a growth temperature of 500°C. The nanowire length increases linearly with growth time over the range of 1 min to 15 min and indicates a growth rate of 2.24 ± 0.23 μm/min for a growth temperature of 500°C. The growth rate was found to be 1.09 ± 0.24 μm/min at 475°C and increased to 4.58 ± 0.77 μm/min at 525°C. It should be noted that the growth rate observed for this study is significantly higher than published reports for MOCVD growth of GaSb nanowires.[8,10] The increase in growth rate is most likely due to the higher metalorganic mole fractions used in this study as well as differences in the growth environment of the hot-wall versus cold-wall MOCVD reactor. In the work of Jeppsson et al.[10] metalorganic molar fractions on the order of 2×10^{-5} to 8×10^{-5} were used, which resulted in GaSb nanowire growth rates in the range of 10 nm/min to 30 nm/min at ~470°C. In contrast, TMGa and TMSb mole fractions of $\sim 1 \times 10^{-2}$ were used in the present study, which is likely responsible for the ~100-fold increase in growth rate that was observed. The growth rate dependence on temperature is shown in Fig. 2b over the temperature range from 475°C to 525°C. The activation energy was determined to be 30.5 ± 5.1 kcal/mol, which is similar to the value of 32.7 kcal/mol reported by Jeppsson et al. at a V/III ratio of 1.2.[10] Activation energies for GaSb thin-film deposition have been reported to range from 19.3 kcal/mol to 54 kcal/mol, depending on the study.[14,16–18] In this case, thermal decomposition of TMSb is assumed to be the rate-limiting step at lower temperatures due to the higher decomposition temperature of TMSb compared with TMGa. The activation energy measured in this study for GaSb nanowire growth is within the range of reported activation energies for GaSb thin-film deposition, suggesting that the rate-limiting step is similar in both cases.

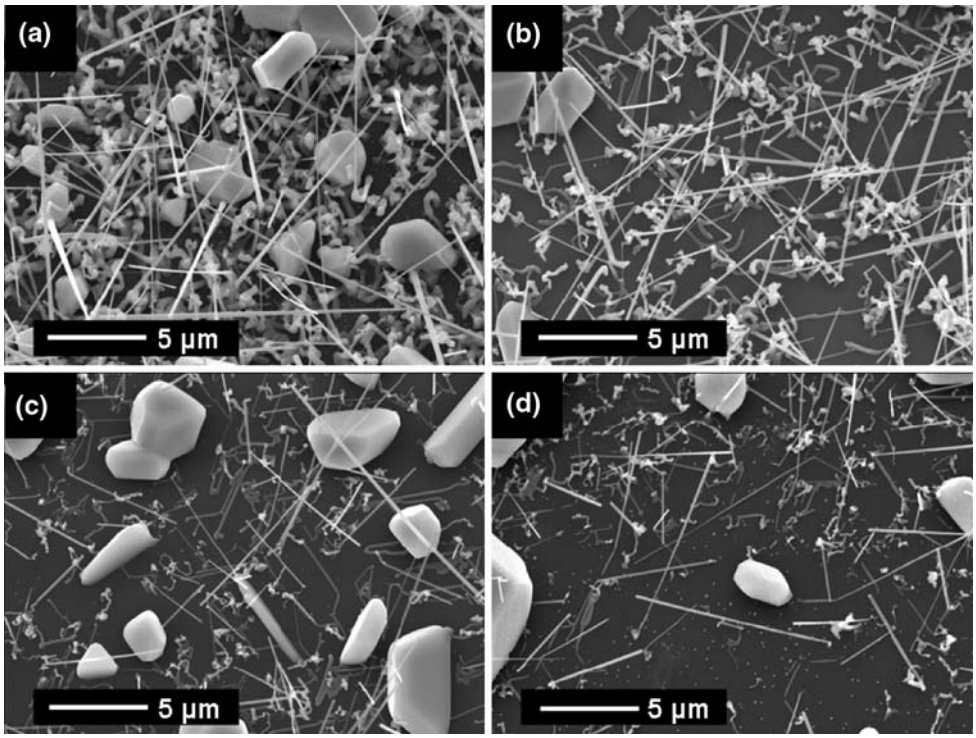

Fig. 3. SEM images of GaSb nanowire growth at V/III ratios of (a) 0.5, (b) 1, (c) 1.5, (d) and 2. Growth conditions: 500°C, 100 Torr, 100 sccm H_2, and 5 min growth.

In order to investigate the effect of V/III ratio on nanowire growth, a series of experiments were carried out at a growth temperature of 500°C and process pressure of 100 Torr. The V/III ratio was varied from 0.5 to 2 while maintaining an overall metalorganic flow rate of 2 sccm. All growths were completed in 5 min, and the results for the sample grown at a V/III ratio of 1 was used as the standard for comparison purposes (Fig. 3b). Decreasing the V/III ratio to 0.5 (Ga rich) led to an increase in the nanowire density along with a higher density of GaSb crystallites (Fig. 3a). Growth in a Ga-rich regime also led to noticeable tapering of the GaSb nanowires. For this condition, the tip diameter was approximately 100 nm, while the base diameter was on the order of 300 nm. It is suspected that growth under Ga-rich conditions leads to Ga droplet formation on the surface of the nanowires, thereby promoting thin-film deposition on the sidewalls.[16]

On the other hand, increasing the V/III ratio (Sb rich) led to a noticeable decrease in the nanowire density (Fig. 3c and d). Based on these findings, it is believed that the nucleation and growth of GaSb nanowires are more dependent on the supply of Ga (TMGa) to the substrate at higher temperatures. This is further supported by examining the effect of V/III ratio on the average nanowire length (growth rate) for each condition. Decreasing the V/III ratio (Ga rich) only led to a slight decrease in the nanowire length from 13.9 ± 2.7 μm to 11.4 ± 1.7 μm. However, increasing the V/III ratio (Sb rich) resulted in a significant decrease in the average nanowire length to 7.7 ± 2.8 μm for a V/III ratio of 1.5 and 8.4 ± 1.7 μm for a V/III ratio of 2. Although the average nanowire length is slightly higher for a V/III ratio of 2, it should be noted that the standard deviation is lower for this case. The data suggests that growth in an Sb-rich regime leads to an excess of Sb, which hinders GaSb nanowire growth compared with in a Ga-rich regime. Overall, however, GaSb nanowire growth near a V/III ratio of 1 appears to be ideal, which is consistent with previous studies.[4,14]

Structural and Chemical Composition

Initial TEM analysis was performed on a sample grown at 500°C, 100 Torr, and V/III ratio of 1. A low-magnification image of a GaSb nanowire grown under these conditions is displayed in Fig. 4a. From the selected-area diffraction pattern (inset to Fig. 4a), the nanowires were found to have the zincblende structure. A portion of the nanowires, such as the one shown in Fig. 4a, were observed to possess twin boundaries that extended the length of the nanowires. Figure 4b, on the other hand, shows a high-resolution TEM image of a GaSb nanowire without a twin. A sharp interface between the GaSb nanowire and the Au catalyst is evident, and the catalyst is approximately the same size as the nanowire. There also appears to be a thin oxide layer on the order of 3 nm to 4 nm surrounding the nanowire.

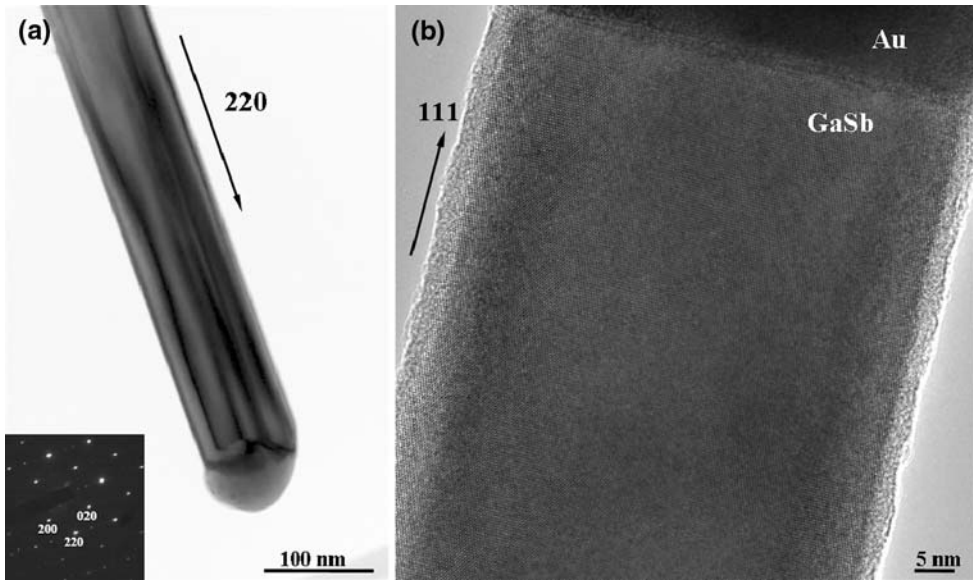

Fig. 4. (a) Low-magnification and (b) high-resolution TEM images of GaSb nanowires. Inset to (a) is an electron diffraction pattern. The sharp interface between the nanowire and seed particle can be seen in (b). Growth conditions: 500°C, 100 Torr, 1 sccm TMGa, 1 sccm TMSb, 100 sccm H_2, and 5 min growth.

Extensive analysis of this sample was performed to determine the average diameter and growth direction of the nanowires on a collection of 58 and 40 nanowires, respectively. The average nanowire diameter was 91 ± 31 nm, which is significantly larger than the original 50-nm-diameter Au catalyst. An increase in the nanowire diameter would be expected due to the volume change necessary to incorporate Ga and Sb atoms within the catalyst. The predominant growth direction (~68% of the nanowires) was found to be [111], while [220] was also found to be a common growth direction (~23% of the nanowires). Other growth directions observed were [331], [221], [112], and [104].

XEDS was utilized to examine the constituents present in the seed particle and the homogeneity of the nanowire. Composition line profiles were taken along the axis (A–A′) of the nanowire (Fig. 5a). The Ga and Sb peak intensities remain constant until reaching the interface between the seed particle and the nanowire. As the line scan continues into the catalyst, the Ga peak intensity does not change; however, a decrease in the Sb intensity is observed along with a sharp increase in the Au intensity (Fig. 5b). Emispec ES Vision Software (FEI Company, Hillsboro, OR) was used in order to determine the composition ratio of Au, Ga, and Sb in the catalyst. For this sample, the catalyst was found to consist of 43 at.% to 45 at.% Au, 14 at.% to 17 at.% Sb, and 40 at.% to 42 at.% Ga. The presence of significant fractions of Au, Ga, and Sb in the catalyst suggests that the VLS mechanism is responsible for the GaSb nanowire growth. The high concentration of Ga and Sb within the catalyst also aids in explaining why a significant increase in the nanowire diameter was observed with respect to the initial 50-nm Au nanoparticle.

Upon completion of the initial TEM analysis, additional studies were carried out on nanowire samples grown at the same conditions along with samples grown at reactor pressure of 100 Torr but utilizing different growth temperatures and V/III ratios. In general, the structural properties and catalyst composition of the nanowires were not found to vary significantly from sample to sample. It should be noted, however, that XEDS analysis identified the presence of two additional types of catalyst particles within a given sample. For each case, a variation in the seed particle composition was observed. An example of the second type of catalyst particle is shown in Fig. 6a. In this case, the GaSb nanowires were found to be bicrystalline, with a seed particle consisting of two grains, labeled A and B. The phase contrast in the lower half of the nanowire indicates the twin boundary of the bicrystalline nanowire and coincides well with the interface between the two grains in the catalyst. In order to investigate the nature of the catalyst particle, a composition line scan was performed through grains A and B along the *y*-axis (Fig. 6c). The line scan was initiated in grain B, where the Sb peak intensity was approximately four times stronger than the Ga peak intensity. As the beam approached the interface between the two grains, the intensity of the Sb peak dropped while the intensity of the Ga peak rose, indicating that grain B is Sb rich and grain A is Ga rich (Fig. 6e). Grain A was found to consist of ~40 at.% Ga, 55 at.% to 60 at.% Au, and 0 at.% to 5 at.% Sb. Grain B, on the other hand, was found to consist of 2 at.% Ga, 43 at.% Au, and 55 at.% Sb.

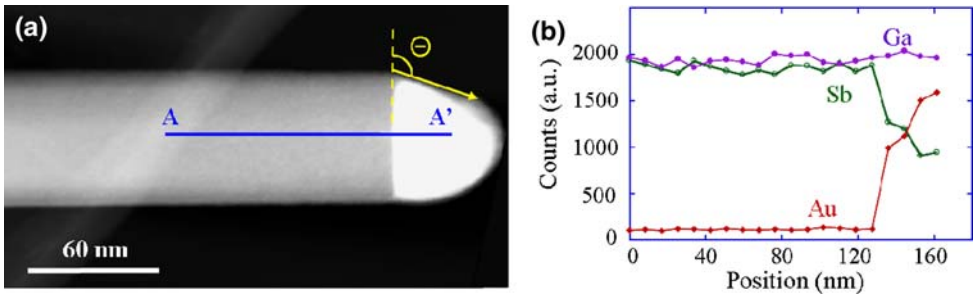

Fig. 5. (a) High-angle annular dark-field (HAADF) STEM image of a GaSb nanowire. (b) XEDS line profile along the axis of the nanowire. Yellow arrow indicates contact angle. Growth conditions: 500°C, 100 Torr, 1 sccm TMGa, 1 sccm TMSb, 100 sccm H_2, and 5 min growth.

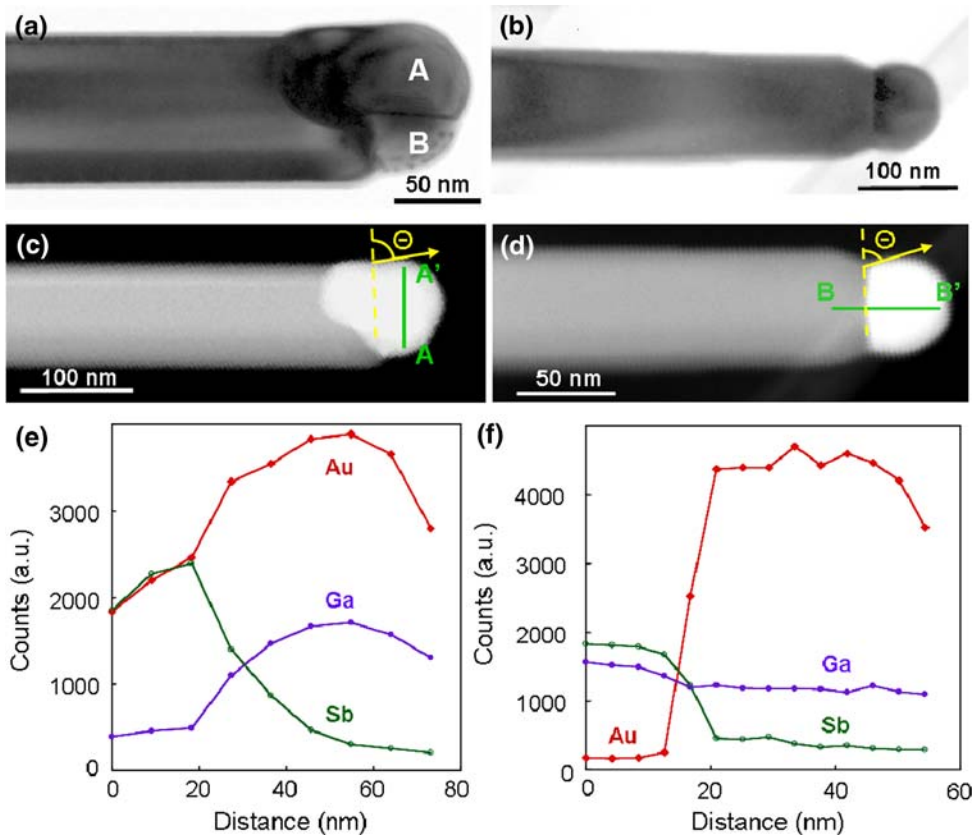

Fig. 6. (a) Bright-field TEM and (c) HAADF STEM images of a bicrystalline GaSb nanowire grown at temperature of 475°C with a catalyst particle containing two grains (A and B). (b) Bright-field TEM and (d) HAADF STEM images of a GaSb nanowire grown at V/III ratio of 2. (e, f) Composition line profiles of the catalyst through A–A′ and B–B′, respectively. Yellow arrows indicate contact angles.

An example of the third type of seed particle is provided in Fig. 6b. In the bright-field TEM image, the GaSb nanowire was found to have a pronounced neck below the seed particle. A similar necking region has been observed previously in the growth of GaAs nanowires by chemical beam epitaxy.[19] For GaAs nanowire growth, the formation of the necking region was attributed to excess Ga within the catalyst reacting with arsenic from the arsine gas as the sample cooled down. The diameter decrease resulted from the volume change in the catalyst as it was depleted of Ga. XEDS was employed to profile the composition along the length of the necked region, as shown in Fig. 6d. A slight decrease was observed in the Ga peak on moving from the nanowire into the catalyst, while a significant decrease in the intensity was found for Sb (Fig. 6f). The seed particle in this case was found to consist of 24 at.% to 28 at.% Ga, 0 at.% to 2 at.% Sb, and 71 at.% to 75 at.% Au. Not only was there a decrease in the concentration of Sb compared with previous studies (14 at.% to 17 at.% and 55 at.% Sb), but there was also a decrease in the typical concentration found for Ga (40 at.% Ga). Based on these results, it is believed that the necking region forms as a result of diffusion of both Ga and Sb out of the catalyst during the cooling period. The change in nanowire diameter in the necking region is

consistent with the volume change of the seed particle as the precipitation reaction takes place.

Summarizing the previous results, there appear to be three distinct seed particle compositions, which are independent of the GaSb nanowire growth conditions. For simplification purposes, the seed particles will be referred to as particles I, II, and III. In the case of particle I, the seed particle was found to consist of 40 at.% to 42 at.% Ga, 14 at.% to 17 at.% Sb, and 43 at.% to 45 at.% Sb. Particle II, on the other hand, was composed of two grains, A and B. Grain A contained 40 at.% Ga, 0 at.% to 5 at.% Sb, and 55 at.% to 60 at.% Au, while grain B consisted of 2 at.% Ga, 55 at.% Sb, and 43 at.% Au. Finally, particle III was found to possess a pronounced necking region below the seed particle, and the seed particle was determined to consist of 24 at.% to 28 at.% Ga, 0 at.% to 2 at.% Sb, and 71 at.% to 75 at.% Au. It should also be noted that, due to the ~2 at.% detection limit of XEDS, it is uncertain whether Sb is present in particle II (grain A) and particle III, and likewise whether Ga is present in particle II (grain B). Selected-area diffraction was carried out in an attempt to identify the phases present in the various catalysts; however, the presence of multiple low-symmetry phases made it difficult to decipher the diffraction patterns.

Therefore, the ternary phase diagram for the Au-Ga-Sb system was utilized in an attempt to identify the phases present in the various catalyst particles. Referring to the ternary Au-Ga-Sb phase diagram,[20,21] which is reconstructed schematically in Fig. 7, the composition of particle I corresponds well with an alloy that lies along a speculative tie-line connecting AuGa to $AuSb_2$, which was previously identified by Tsai et al.[20] using x-ray diffraction. The phases for this alloy were identified to be GaSb, $AuSb_2$, AuGa, and γ'. The γ' phase is believed to be Au_7Ga_3, Au_2Ga, or Au_9Ga_4. Assuming that negligible Sb is present in particle III, this would place the composition of particle III along the Au–Ga axis, which correlates well with the γ' phase.[22]

Particle II, on the other hand, is more difficult to identify due to the presence of multiple grains within the seed particle. Therefore, an assumption is made that grains A and B contain negligible amounts of Sb and Ga, respectively, due to the detection limits of XEDS. As a result, particle II can be described as consisting of an Au-Ga-rich grain (A) and an Au-Sb-rich grain (B), which are believed to have formed due to the phase separation of the seed particle. According to the ternary phase diagram shown in Fig. 7, grain A (IIA) is located in the vicinity of γ' but is less Au rich than γ', while grain B (IIB) is located in the vicinity of $AuSb_2$ but is more Au rich than $AuSb_2$.[22] In an earlier study on the effect of particle size on the composition of Au-Sb alloys, the $AuSb_2$ compound, typically located at 67 at.% Sb, was observed over a range of 52 at.% to

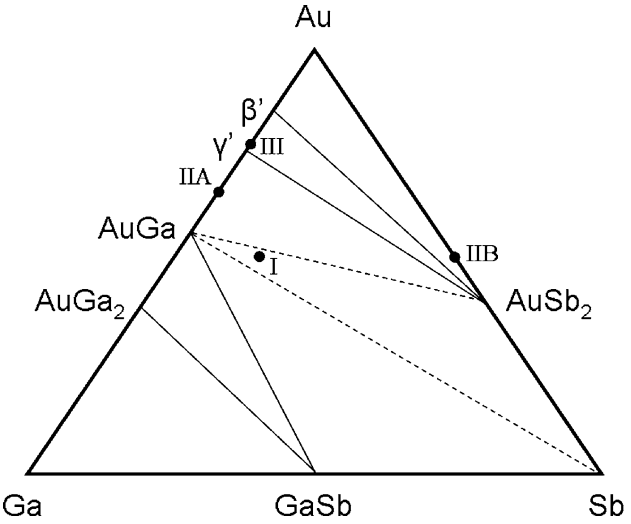

Fig. 7. Schematic of the ternary phase diagram for the Au-Ga-Sb system at 298 K. Solid lines are known pseudobinary tie-lines, while dotted lines are speculative pseudobinary tie-lines. The three catalyst particle compositions have been labeled on the ternary phase diagram as I, II (grains A and B), and III.

77 at.% Sb for nanoscale (up to ~15 nm) particles.[23,24] Therefore, a possible explanation for the composition shift of grain A from γ' and grain B from $AuSb_2$ could be due to a nanoscale size effect, although further studies are obviously required to determine if this would indeed be applicable to the size range of the catalyst particles in this study.

The TEM images shown in Figs. 5 and 6 also suggest that the composition of the catalyst alters the contact angle between the seed particle and the nanowire interface, and that the Sb concentration plays a large role in this behavior. In this case, the contact angle is defined as the angle between the catalyst surface and the plane of the catalyst–nanowire interface, as shown in Figs. 5a and 6c and d. If the seed particle contains higher concentrations of Sb, such as that shown in Fig. 5a for 14 at.% to 17 at.% Sb, the contact angle is close to or greater than 90°, whereas contact angles less than 90° are observed if the concentration of Sb in the catalyst is relatively low, such as that shown in Fig. 6b and d where the Sb concentration was 0 at.% to 2 at.%.

The change in contact angle can be explained based on the differences in the surface energy of the catalyst particle as the Sb concentration is varied. Following the methodology used to describe wetting behavior on a solid surface,[25] mechanical equilibrium among the vertical components of the vapor–liquid surface tension (γ_{LV}), the vapor–solid surface tension (γ_{SV}), and the liquid–solid interfacial tension (γ_{LS}) yields the equation

$$\sin\theta = \frac{\gamma_{SV}}{\gamma_{LV}}, \tag{1}$$

where θ, the contact angle, is defined as the angle between the vapor–liquid surface tension vector and

the plane of the liquid–solid interface. While a more detailed approach is required to calculate exact values for the surface tension of liquid alloy mixtures, the effect of Sb on γ_{LV} can be qualitatively assessed by comparing the values for the pure components (Au = 1.140 J/m^2, Ga = 0.677 J/m^2, Sb = 0.355 J/m^2) and the binary mixture (GaSb = 0.520 J/m^2).[26–28] Assuming that γ_{SV} is a constant, irrespective of growth conditions, the addition of Sb to the liquid catalyst would result in a reduction in γ_{LV} and therefore an increase in the contact angle. Although the mechanical equilibrium model assumed a liquid-phase catalyst, the predicted trends in contact angle are in qualitative agreement with the contact angles of the solid-phase catalysts observed from TEM analysis. The type I catalyst (Fig. 5a), which has a larger concentration of Sb, exhibits a larger contact angle than the type III catalyst (Fig. 6b and d), which contains primarily Au and Ga. The change in catalyst composition and contact angle is also expected to impact the nanowire growth, as predicted by Nebol'sin and Shchetinin[29]; however, *in situ* growth studies are required to investigate these effects experimentally.

Electrical Measurements

Four-point resistivity and gate-dependent current–voltage measurements were performed on 17 GaSb nanowires grown at 500°C, 100 Torr, 1 sccm TMGa, and 1 sccm TMSb. An SEM image of the test-bed structure is shown in Fig. 8a. Current–voltage characteristics measured between S and D electrodes separated by 1.6 μm for nominally undoped GaSb nanowires are shown in Fig. 8b. A linear I–V dependence was observed with a ~1 μA to 2 μA current at ±2.0 V. In order to eliminate contributions from contact resistance, the GaSb nanowire resistance (R_{NW}) was measured using a four-point configuration, where the differential voltage ΔV developed across the two internal voltage probes was divided by the current induced between the two external electrodes. Nanowire resistivity (ρ_{NW}), determined from R_{NW} using dimensions measured of 17 nanowires by field-emission SEM (FESEM), was found to be 0.23 ± 0.18 Ω cm, which is similar to values reported for undoped GaSb thin films[14] and nanowires.[9] The variation of current in the nanowires as a function of back-gate voltage (V_{DS} = 0.1 V) is shown as an inset to Fig. 8b. The current decreases with increasing positive back-gate bias, indicating that the nominally undoped GaSb nanowires are p-type. Independent of the growth technique, undoped GaSb is observed to be p-type in nature,[5] which is consistent with the results obtained for the GaSb nanowires. Extensive work has been performed to investigate the nature of the unintentional p-type doping, and a native defect associated with excess Ga or a deficiency of Sb in GaSb has been linked to this characteristic.[30,31] The complex has been

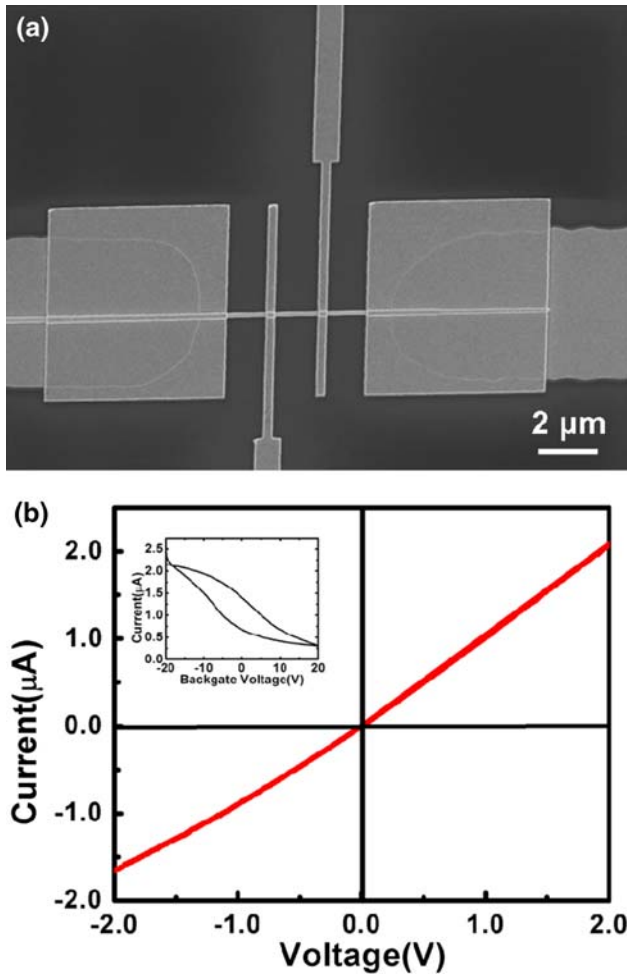

Fig. 8. (a) FESEM image of back-gated test-bed structure. (b) Four-point resistivity and gate-dependent current–voltage measurements (inset) of GaSb nanowires.

identified as a $V_{Ga}Ga_{Sb}$ center where a Ga atom occupies an Sb site due to an Sb vacancy and leaves a Ga vacancy behind. Carbon incorporation due to the relatively low growth temperatures employed may also contribute to the p-type conductivity.[32] In addition to native acceptor defects in the bulk, oxygen and metal impurities on the surface of GaSb have been shown to pin the Fermi level at the surface near the valence-band maximum.[33–35] These results are consistent with the linear current–voltage characteristics (Fig. 8b) obtained for the unpassivated GaSb nanowires examined in this study.

PL Measurements

PL measurements were carried out on the GaSb nanowire samples grown at various V/III ratios to further investigate dopant and deep-level states in the material. Samples for this study were grown at V/III ratios of 0.5, 1, 1.5, and 2, and the resulting PL spectra obtained at low laser powers are shown in Fig. 9a. PL measurements for the sample grown at a

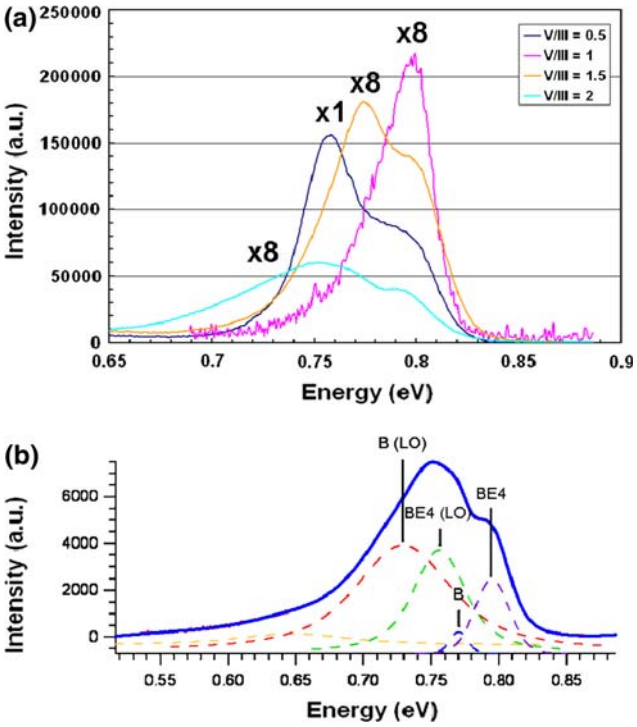

Fig. 9. (a) PL measurements of GaSb nanowires grown at V/III ratios of 0.5, 1, 1.5, and 2. The sample grown at V/III ratio of 1 was completed with laser power of 15 mW and temperature of 3.5 K. The other samples were analyzed at laser power of 12 mW and temperature of 5 K. The intensities of the PL for samples grown at V/III ratios of 1, 1.5, and 2 were multiplied by a factor of 8 for comparison purposes. (b) PL spectrum at 5 K of GaSb nanowire sample with V/III ratio of 2. The dotted peaks are peak fits for the various transitions and are offset from the axis. The blue peak is the overall fit for the spectrum. The red underlying spectrum is the original curve based on the PL data.

V/III ratio of 1 were carried out at a laser power of 15 mW and temperature of 3.5 K. The rest of the samples were analyzed at a laser power of 12 mW and temperature of 5 K. The intensities of the PL at V/III ratios of 1, 1.5, and 2 were multiplied by a factor of 8 for comparison purposes. It is believed that the high intensity observed at a V/III ratio of 0.5 is due to the higher nanowire density on this sample. In general, the PL peaks are broad and the overall intensity was found to decrease with increasing V/III ratio, which also coincides with a decrease in the nanowire density.

In order to gain a better understanding of the PL spectra, IGOR Pro software was utilized in an attempt to resolve the locations of the underlying peaks for each individual spectrum. An example of the peak fitting is shown in Fig. 9b. The fitted peaks can all be attributed to transitions associated with the native defect ($V_{Ga}Ga_{Sb}$ center) in GaSb, which acts as a residual acceptor.[30,31] The residual acceptor is linked to various peaks including the A peak (777 meV), acceptor B peak (758 meV), and the bound exciton (BE) peaks (796 meV to 805 meV). The resolved peaks shown in Fig. 9b for a sample grown under Sb-rich conditions with a V/III ratio of 2 can be attributed to acceptor B and BE transitions. At a V/III ratio of 0.5 (Ga-rich conditions), transitions associated with the native acceptor (A line) and acceptor B were found to dominate. On the other hand, at a V/III ratio of 1, higher-energy transitions (BE peaks) were found to dominate the spectrum and the full-width at half-maximum was reduced, indicating that the GaSb nanowires were of higher optical quality.

Overall, the results suggest that a V/III ratio of 1 is optimal for synthesis of GaSb nanowires. Growth in Ga-rich and Sb-rich regimes leads to significant degradation of optical properties. For GaSb nanowires grown at a V/III ratio of 0.5, the A line (donor–acceptor pair) dominates, because the native defect is enhanced due to deficiency of Sb. On the other hand, growth in an Sb-rich regime minimizes the effect of the residual acceptor but leads to the formation of other defect peaks. GaSb nanowire growth at a V/III ratio near unity, however, leads to dominance of high-energy transitions (BE peaks) with respect to the A line peak. These findings are consistent with the electrical results, which indicated that the samples were *p*-type due to the presence of the native acceptor defect.

CONCLUSIONS

Synthesis of GaSb nanowires by MOCVD was investigated in an isothermal tube reactor, and a narrow window of growth conditions was identified. TEM analysis indicated that the primary growth direction for GaSb nanowire growth was [111]. XEDS revealed that a majority of the nanowires possessed high concentrations of Ga and Sb in the catalyst after growth, supporting a VLS growth mechanism. The composition of the catalyst was observed to vary across the set of nanowires investigated, and the different phases present were explained in terms of the ternary phase diagram for the Au-Ga-Sb system. Four-point resistivity measurements, conducted on individual GaSb nanowires, indicated that the nominally undoped nanowires were *p*-type with resistivity of $0.23 \pm 0.18\ \Omega$ cm. PL measurements revealed the presence of acceptor-related emissions which varied as a function of the V/III ratio used during nanowire growth.

ACKNOWLEDGEMENTS

This work was supported by the National Science Foundation under Grant No. ECS-0093742 and The Pennsylvania State University Materials Research Science and Engineering Center (MRSEC) on Nanoscale Science. Additional support was provided by Illuminex Corp. under an NSF Phase I STTR program (0740336). The TEM work was performed in the electron microscopy facility of the Materials Characterization Laboratory (MCL) at the Pennsylvania State University.

REFERENCES

1. W. Xu, A. Chin, L. Ye, C.-Z. Ning, and H. Yu, *SPIE Proceedings on Electrical and optical characterization of individual GaSb nanowires* (San Jose, 2009).
2. A.H. Chin, S. Vaddiraju, A.V. Maslov, C.Z. Ning, M.K. Sunkara, and M. Meyyappan, *Appl. Phys. Lett.* 88, 163115 (2006).
3. N. Mingo and D.A. Broido, *Phys. Rev. Lett.* 93, 246106 (2004).
4. P.S. Dutta, H.L. Bhat, and V. Kumar, *J. Appl. Phys.* 81, 5821 (1997).
5. R.M. Biefeld, *Mater. Sci. Eng. R Rep.* 36, 105 (2002).
6. A. Lugstein, J. Bernardi, C. Tomastik, and E. Bertagnolli, *Appl. Phys. Lett.* 88, 163114 (2006).
7. S. Vaddiraju, M. Sunkara, A. Chin, C. Ning, and G. Dholakia, *J. Phys. Chem. C* 111, 7339 (2007).
8. Y.N. Guo, J. Zou, M. Paladugu, H. Wang, Q. Gao, H.H. Tan, and C. Jagadish, *Appl. Phys. Lett.* 89, 231917 (2006).
9. M. Jeppsson, K. Dick, H. Nilsson, N. Skold, J. Wagner, P. Caroff, and L.-E. Wernersson, *J. Cryst. Growth* 310, 5119 (2008).
10. M. Jeppsson, K. Dick, J. Wagner, P. Caroff, K. Deppert, L. Samuelson, and L.-E. Wernersson, *J. Cryst. Growth* 310, 4115 (2008).
11. P.A. Smith, C.D. Nordquist, T.N. Jackson, T.S. Mayer, B.R. Martin, J. Mbindyo, and T.E. Mallouk, *Appl. Phys. Lett.* 77, 1399 (2000).
12. J.A. Robinson and S.E. Mohney, *J. Appl. Phys.* 98, 033703 (2005).
13. X. Weng, R.A. Burke, E.C. Dickey, and J.M. Redwing, *J. Cryst. Growth* 312, 514 (2010).
14. A. Subekti, E.M. Goldys, M.J. Paterson, K. Drozdowicz-Tomsia, and T.L. Tansley, *J. Mater. Res.* 14, 1238 (1999).
15. T. Koljonen, M. Sopanen, H. Lipsanen, and T. Tuomi, *J. Electron. Mater.* 24, 1691 (1995).
16. A. Subekti, E.M. Goldys, and T.L. Tansley, *Conference on Growth of Gallium Antimonide (GaSb) by Metalorganic Chemical Vapour Deposition* (IEEE, 1997), pp. 426–429.
17. F. Pascal, F. Delannoy, J. Bougnot, L. Gouskov, G. Bougnot, P. Grosse, and J. Kaoukab, *J. Electron. Mater.* 19, 187 (1990).
18. M.K. Rathi, B.E. Hawkins, and T.F. Kuech, *J. Cryst. Growth* 296, 117 (2006).
19. A.I. Persson, M.W. Larsson, S. Stenstrom, B.J. Ohlsson, L. Samuelson, and L.R. Wallenberg, *Nat. Mater.* 3, 677 (2004).
20. C.T. Tsai and R.S. Williams, *J. Mater. Res.* 1, 352 (1986).
21. W.E. Lui and S.E. Mohney, *J. Electron. Mater.* 32, 1090 (2003).
22. H. Okamoto and T.B. Massalski, eds., *Phase Diagrams of Binary Gold Alloys* (Materials Park, OH: ASM International, 1987).
23. H. Yasuda and H. Mori, *J. Cryst. Growth* 237–239, 234 (2002).
24. H. Yasuda, M. Takeguchi, K. Mitsuishi, M. Tanaka, M. Song, K. Furuya, and H. Mori, *J. Electron. Microsc.* 51, S215 (2002).
25. M. Ohring, *Materials Science of Thin Films*, 2nd ed. (New York: Academic, 2002).
26. S.C. Hardy, *J. Cryst. Growth* 71, 602 (1985).
27. V.K. Kumikov and K.B. Khokonov, *J. Appl. Phys.* 54, 1346 (1983).
28. A. Tegetmeier, A. Croll, A. Danilewsky, and K.W. Benz, *J. Cryst. Growth* 166, 651 (1996).
29. V.A. Nebol'sin and A.A. Shchetinin, *Inorg. Mater.* 39, 899 (2003).
30. Y.J. Van Der Meulen, *J. Phys. Chem. Solids* 28, 25 (1967).
31. W.G. Hu, Z. Wang, B.F. Su, Y.Q. Dai, S.J. Wang, and Y.W. Zhao, *Phys. Lett. A* 332, 286 (2004).
32. K. Yamamoto, H. Asahi, K. Inoue, K. Miki, X.F. Liu, D. Marx, A.B. Villaflor, K. Asami, and S. Gonda, *J. Cryst. Growth* 150, 853 (1995).
33. P.W. Chye, I. Lindau, P. Pianetta, C.M. Garner, C.Y. Su, and W.E. Spicer, *Phys. Rev. B* 18, 5545 (1978).
34. P.W. Chye, T. Sukegawa, I.A. Babalola, H. Sunami, P. Gregory, and W.E. Spicer, *Phys. Rev. B* 15, 2118 (1977).
35. W.E. Spicer, P.W. Chye, P.R. Skeath, C.Y. Su, and I. Lindau, *J. Vac. Sci. Technol.* 16, 1422 (1979).